Signalome-wide mapping of the NFκB pathway in T-cells reveals novel targets for immunotherapy

Joseph Clarke[1], Haoqi Chen[2], Cristina Tormo Garcia[1], Ewa Basiarz[3], Mateusz Kotowski[1], Ana Mafalda Santos[1], Mai T Voung[1], Paige Sherman[1], Jia Xin Li[1], Christopher J Tape[3#], Simon J Davis[1#], Evangelia Petsalaki[2#], Sumana Sharma[1#]

[1]Radcliffe Department of Medicine, John Radcliffe Hospital, University of Oxford, Oxford, OX3 9DS, United Kingdom

[2]European Molecular Biology Laboratory, European Bioinformatics Institute (EMBL-EBI), Wellcome Genome Campus, Hinxton, Cambridgeshire, CB10 1SD, United Kingdom

[3]Cell Communication Laboratory, Department of Oncology, University College London Cancer Institute, 72 Huntley Street, London, WC1E 6DD, United Kingdom

[#]Correspondence should be addressed to:

sumana.sharma@rdm.ox.ac.uk

petsalaki@ebi.ac.uk

simon.davis@imm.ox.ac.uk

c.tape@ucl.ac.uk

Abstract

Cell signalling networks govern fundamental cellular processes yet remain incompletely defined. Moreover, what is known is biased toward a limited subset of well-characterised components. Phosphoprotein-based interrogation methods, including mass spectrometry and targeted phosphosite panels, have limited utility in physiological settings dependent on cell–cell interactions because the signalling fluxes can be difficult to detect despite producing robust functional responses. Here we developed a perturbation-based experimental framework that infers signalling pathway architecture using quantitative functional outputs rather than direct measurements of effector state, e.g., phosphorylation levels. Using antigen-specific, NF-κB–GFP reporter-expressing transformed T-cells co-cultured with cellular targets, we performed an arrayed CRISPR–Cas9 screen targeting a curated signalome of kinases, phosphatases, adaptor and scaffolding proteins, totalling 706 genes. Quantitative effect-size profiling recovered canonical T-cell receptor regulators and revealed unequal, family-specific patterns of control over NF-κB activation. Comparing T-cell stimulation with low- and high-affinity antigen uncovered signal-strength-dependent buffering of proximal signalling nodes, exemplified by reduced sensitivity to perturbation of *LCK* under high-intensity stimulation. Targeted perturbation in primary human $CD8^+$ T-cells validated our findings and identified *TRRAP* and *CTDSPL2* as negative regulators of T-cell effector output, whose disruption enhanced cytotoxicity, degranulation, and cytokine production in both polyclonal and TCR-engineered T cells. Together, these results establish a scalable strategy for mapping signalling pathway architecture in the setting of physiological T-cell activation.

Introduction

Cellular signalling is crucial for fundamental processes such as growth, proliferation, differentiation, survival, metabolism, and specialised effector responses. Although powerful technologies such as CyTOF, LC–MS-based phosphoproteomics, and targeted phospho-panels have significantly advanced our ability to interrogate signalling events, our understanding of cellular signalling network structure and regulation remains incomplete. Moreover, current knowledge is disproportionately focused on a limited subset of well-studied components, leaving large portions of the signalling landscape poorly characterised.(*1*). This bias is particularly pronounced for kinases and phosphatases, the principal enzymatic drivers of signal transduction, for which an estimated 30-50% of cellular targets remain unknown, indicating that large regions of the signalling landscape remain unexplored (*2*).

Most contemporary approaches to studying signalling rely on direct measurement of molecular intermediates, most commonly phosphorylation events detected by antibody-based assays or mass spectrometry-based phosphoproteomics. Advances in enrichment-based LC-MS have enabled increasingly global profiling of signalling states (*3*–*8*), and these approaches have been extended through integration with genetic or pharmacological perturbations to infer causal relationships, exemplified by resources such as the Connectivity Map (CMap) (*9*). Despite these advances, molecular readout-based approaches remain limited in their ability to capture signalling behaviour under physiological conditions. They are biased toward abundant or highly dynamic phosphorylation events, require large numbers of cells, and rely heavily on curated pathway annotations for interpretation, reinforcing existing knowledge rather than revealing new regulatory logic. Consequently, signalling components that exert modest, distributed, or context-dependent effects on pathway output may be systematically overlooked.

These limitations are particularly pronounced in systems where signalling is spatially constrained and dependent on direct cell–cell interactions. Most phosphoproteomic and

kinase-activity-based studies are performed on bulk cell lysates, restricting their applicability in such contexts. T-cell activation exemplifies this challenge: apart from a small number of SILAC-based co-culture studies (*10–12*), much of the available signalling data relies on supraphysiological stimulation applied outside native cellular contexts to generate detectable responses (*5*, *13*). Single-cell approaches such as mass cytometry (CyTOF) partially address population averaging (*14–17*). However, these approaches also encounter biological limits. In direct T cell–target cell interactions, single-cell mass cytometric analyses reveal remarkably limited signalling flux, often indistinguishable from unstimulated states, in contrast to pharmacological induced T-cell activation (*18*). Notably, despite these modest detectable fluxes, T cells mount robust functional responses, indicating that phosphoprotein-based measurements fail to capture physiologically relevant signalling dynamics.

In contrast, functional outputs integrate signalling information over time and across molecular layers. This suggests an alternative strategy for interrogating signalling networks: rather than measuring signalling intermediates directly, signalling architecture can be inferred by systematically perturbing signalling components and quantifying their impact on downstream functional outputs.

Here, we implement this concept through a perturbation-based framework that reconstructs signalling dependencies directly from functional readouts. By combining arrayed CRISPR-Cas9-mediated gene disruption with a quantitative NF-κB reporter assay, we systematically interrogate the contribution of kinases, phosphatases, and adaptor proteins to signalling pathway transmission, and subsequent transcription factor activity, in a physiologically relevant, cell–cell interaction context. This approach enables quantitative assessment of graded effects across hundreds of signalling components, revealing how control is distributed across a signalling network rather than identifying only a small number of essential nodes.

Applying this strategy to T-cell receptor signalling, we generate a functional dependency map of NF-κB activation that reveals hierarchical control, distributed engagement across signalling

93 families, and context-dependent buffering of proximal signalling nodes as a function of ligand
94 affinity. Extending these findings to primary human $CD8^+$ T cells, we identify previously
95 unrecognized negative regulators of T-cell function, including TRRAP and CTDSPL2, whose
96 disruption enhances cytotoxic activity and effector responses. Together, this work establishes
97 a generalisable framework for reconstructing signalling architecture from functional outputs in
98 physiological contexts.

99 Results

100 A functional 1G4-TCR^+ Jurkat NF-kB reporter system enables analysis of T-cell
101 receptor signalling under physiological stimulation conditions.

102 To enable systematic interrogation of T-cell signalling through functional outputs, we
103 generated a Jurkat T-cell reporter line in which NF-κB activity is monitored via GFP expression
104 downstream of antigen-specific T-cell receptor (TCR) engagement. NF-κB was selected as a
105 core transcriptional output of T-cell activation, integrating signals from multiple proximal and
106 distal signalling pathways. Jurkat cells were first engineered to stably express an NF-κB-driven
107 GFP reporter (**Supplementary Fig. 1A-B)**. To ensure antigen-specific activation, endogenous
108 TCR expression was ablated by CRISPR targeting of *TRAC* and *TRBC*, and cells were
109 subsequently transduced with lentivirus encoding the 1G4 TCR (**Supplementary Figure 1C**),
110 which recognizes the cancer-testis antigen NY-ESO-$1_{157-165}$ (henceforth referred to simply as
111 NY-ESO-1) peptide presented by HLA-A*02:01, followed by introduction of constitutive Cas9
112 expression to facilitate CRISPR-Cas9-mediated genetic perturbation (**Supplementary Fig.
113 1D**).
114
115 This configuration establishes a defined receptor-ligand interaction that mimics physiological
116 T-cell-target cell engagement. When co-cultured with A375 melanoma cells pulsed with NY-
117 ESO-1 peptides, 1G4-TCR^+ Jurkat reporter cells exhibited robust NF-κB–dependent GFP

118 induction, whereas TCR-deficient parental cells remained unresponsive (**Fig. 1A–C**). Upon
119 the use of NY-ESO-1 altered peptide ligands (6T, 3Y, 3I and 9V) to initiate Jurkat T-cell
120 activation, GFP expression scaled with peptide affinity, demonstrating sensitivity across a
121 physiologically relevant range of TCR stimulation strengths (**Fig. 1B,C**).

122 To confirm that reporter activation reflected canonical TCR signalling, we genetically disrupted
123 key proximal signalling components. CRISPR-mediated targeting of established TCR
124 signalling mediators, including *LCP2* and *ZAP70*, significantly reduced NF-κB reporter activity
125 upon stimulation with both high- and low-affinity antigen (**Fig. 1D**). These results confirm that
126 NF-κB reporter activation depends on intact TCR-proximal signalling.

127 Together, these data establish a genetically tractable, antigen-specific Jurkat reporter system
128 that reliably converts physiologically relevant TCR engagement into a quantitative functional
129 readout of NF-κB activation. This platform provides a robust foundation for systematic
130 perturbation-based analysis of signalling dependencies in a cell–cell interaction context,
131 where direct phosphoprotein measurements are known to be challenging.

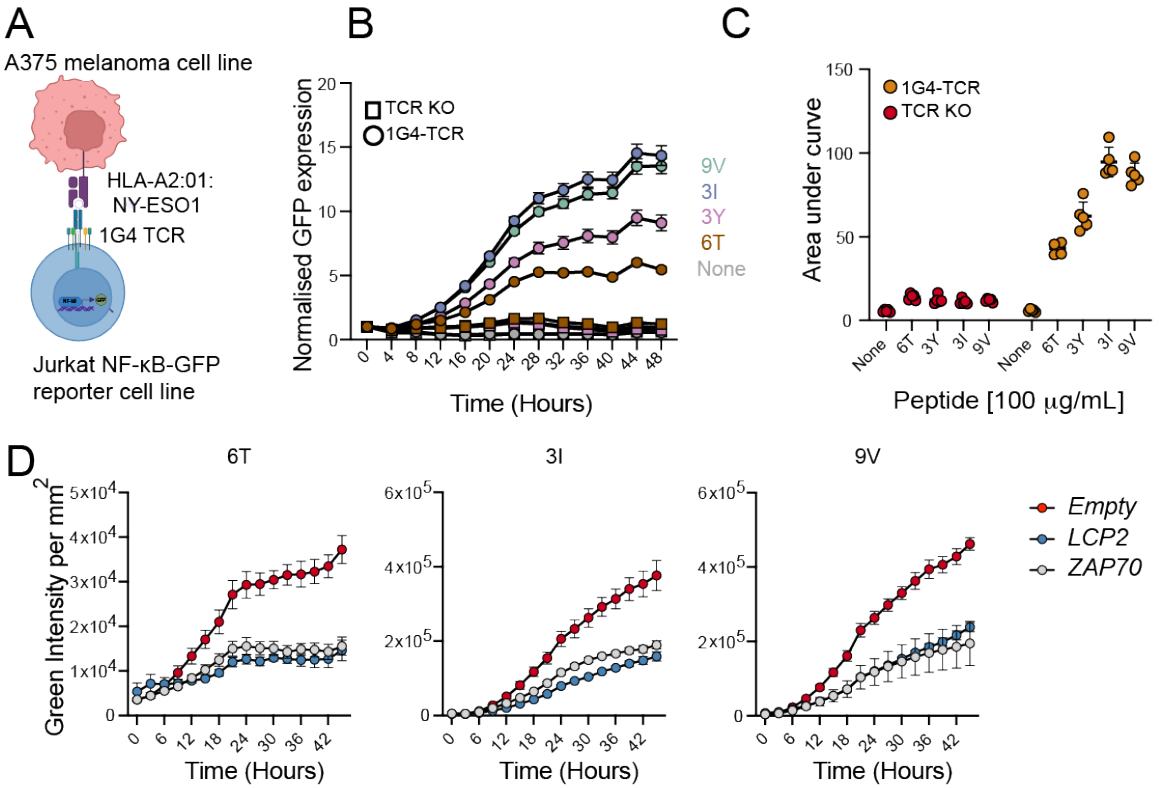

Figure 1: Establishing a peptide:MHC specific cell-cell interaction system to report functional activity of NFkB in T cells A: Schematic representing the co-culture system between Jurkat-NFkB-GFP reporter cell lines expressing the 1G4-TCR, and A375 melanoma cells pulsed with NY-ESO-1 peptides. **B:** Time course IncuCyte measurements of NFkB-GFP intensities from either 1G4-TCR^{+} Jurkat reporter lines (filled circles) or TCR-KO parental lines (filled squares). All NY-ESO-1 altered peptide ligands were used at final concentrations of 100µg/mL. **C:** Area under the curve (AUC) analysis of the data shown in panel B. **D:** Lentiviral sgRNA targeting of key TCR-signalling components *LCP2* or *ZAP70* in 1G4-TCR^{+} Jurkat reporters prevents GFP expression upon co-culture with NY-ESO-1 peptide pulsed A375 melanoma cells. All peptides were used at final concentrations of 100µg/mL, and time course GFP measurements were performed via IncuCyte imaging. All data shown from a minimum of three independent experiments.

A signalome-wide CRISPR-Cas9 screen reveals a quantitative map of NF-κB signalling in T cells

To enable systematic interrogation of T-cell signalling, we first defined a comprehensive "signalome" comprising kinases, phosphatases, and key adaptor proteins. We combined a curated list of 556 human kinases with 136 protein phosphatases defined by the HUGO Gene

152 Nomenclature Committee (*19*), and filtered this set for genes expressed across multiple
153 immune and cancer cell models using bulk RNA-seq data from Cell Model Passports (TPM >
154 0.3; Jurkat, MOLT-4, Daudi, THP-1, and two colorectal cancer organoids) (*20*). To further
155 enrich for signalling components relevant to T cells, we included genes annotated in KEGG
156 pathways associated with TCR signalling, JAK-STAT, calcium signalling, actin regulation,
157 phosphatidylinositol signalling, and MAPK signalling (*21*), as well as all genes encoding for
158 SH2 domain-containing proteins, to ensure coverage of adaptor and scaffolding molecules.
159 This yielded a final library of 706 genes, each targeted with two sgRNAs for CRISPR-Cas9-
160 mediated perturbation (**Supplementary Table 1**).
161
162 To place this signalome in the context of existing knowledge, we integrated transcriptional and
163 perturbation-based datasets from diverse T-cell contexts. Analysis of published expression
164 datasets spanning multiple activation timepoints in $CD8^+$ and pan-T cells (*22–25*) revealed
165 that 446 signalome genes are dynamically regulated at the transcriptional level (**Fig. 2A;**
166 **Supplementary Table 2**). In parallel, we mapped hits from published genome-wide CRISPR
167 loss-of-function and gain-of-function screens in T cells (*26–29*) onto the signalome (**Fig. 2B;**
168 **Supplementary Table 2**). Across these datasets, 64 genes were identified in loss-of-function
169 screens and 49 in gain-of-function screens. Genes implicated by CRISPR perturbation were
170 significantly enriched for genes encoding SH2-domain-containing proteins ($p = 2x10^{-5}$, Fisher's
171 exact test), underscoring their central role in T-cell signalling. Notably, 37 genes that were not
172 transcriptionally regulated nonetheless exhibited functional effects in CRISPR screens,
173 including seven core T-cell signalling genes encoding for SH2-domain-containing proteins
174 (CBLB, GRB2, ZAP70, SLA2, CBL, LCP2, VAV1), whereas many transcriptionally regulated
175 signalling genes were not detected in pooled CRISPR screens, highlighting potential gaps in
176 existing perturbation-based maps (**Fig. 2A,B**).
177
178 We next performed a signalome-wide, arrayed CRISPR perturbation screen to directly quantify
179 the contribution of each component to NF-κB activation. 1G4-TCR^+ Jurkat reporter cells were

180 transduced with individual sgRNAs and stimulated through cell–cell co-culture with peptide-
181 pulsed target cells. In total, ~1,500 sgRNAs targeting ~700 genes were assayed in 96-well
182 format across 13 experimental batches (**Fig. 2C**). Each batch included internal controls,
183 including an empty sgRNA vector and sgRNAs targeting known TCR signalling components
184 (*LCP2, ITK*), enabling normalization of gene-level effects based on GFP signal area under the
185 curve (AUC) relative to empty controls and an internal positive control to assess the editing
186 efficiency (see details in **Methods**).
187
188 The screen showed high technical robustness. Independent sgRNAs targeting the same gene
189 exhibited strong concordance, with ~80% of guide pairs showing consistent effect direction
190 (**Fig. 2D; Supplementary Figure. 2A**). Gene-level effects were highly correlated for T-cell
191 stimulation with low-affinity (6T) and high-affinity (9V) antigens (Spearman $\rho = 0.93$), indicating
192 that the core signalling architecture governing NF-κB activation is largely conserved across
193 stimulation strengths (**Fig. 2E**). Most genes clustered near the identity line, whereas a subset
194 showed context-dependent deviations. Notably, disruption of *LCK* strongly attenuated NF-κB
195 activation under weak stimulation but had a markedly reduced effect under high-affinity
196 stimulation (**Supplementary Figure. 2B**), consistent with partial bypass or compensation at
197 higher signalling strength (*30*, *31*).

198 To characterise the global structure of signalling control, we ranked genes by their mean effect
199 size across both conditions. The distribution was strongly skewed toward negative effects,
200 consistent with depletion-driven signalling dependencies rather than enrichment effects (**Fig.**
201 **2F**). Canonical TCR signalling components, including *LCK, ZAP70, ITK, and LCP2*, ranked
202 among the strongest negative regulators, validating the ability of this approach to recover core
203 pathway architecture (**Fig. 2F**). TCR-specific signalling was among the highest-ranked
204 pathways in the enrichment analysis, suggesting that the screen successfully recapitulated
205 known genes while also assigning quantitative scores to signalome genes involved in
206 regulating the NF-κB pathway (**Supplementary Figure 2C**).

207 We next examined how signalling control was distributed across protein families by comparing
208 effect size distributions within each family (**Fig. 2G**). All families contributed to NF-κB
209 regulation, but with distinct patterns. SH2-domain-containing proteins exhibited broad effect
210 size distributions, indicating distributed engagement of multiple family members. In contrast,
211 MAP kinase contributions were concentrated in a small number of nodes, leading towards
212 ERK1/2 (*MAPK3/MAPK1*) and p38α (*MAPK14*) (**Fig 2F, H**). These patterns suggest that NF-
213 κB signalling integrates both distributed adaptor-mediated control and more focal kinase
214 bottlenecks, rather than being uniformly dominated by single components. Based on these
215 quantitative dependencies, we reconstructed a data-driven network representation of NF-κB
216 regulation, capturing hierarchical patterns of control, characterized by a small number of high-
217 impact nodes alongside broadly distributed contributions from adaptor families (**Fig. 2H;**
218 **Supplementary Table 3**).

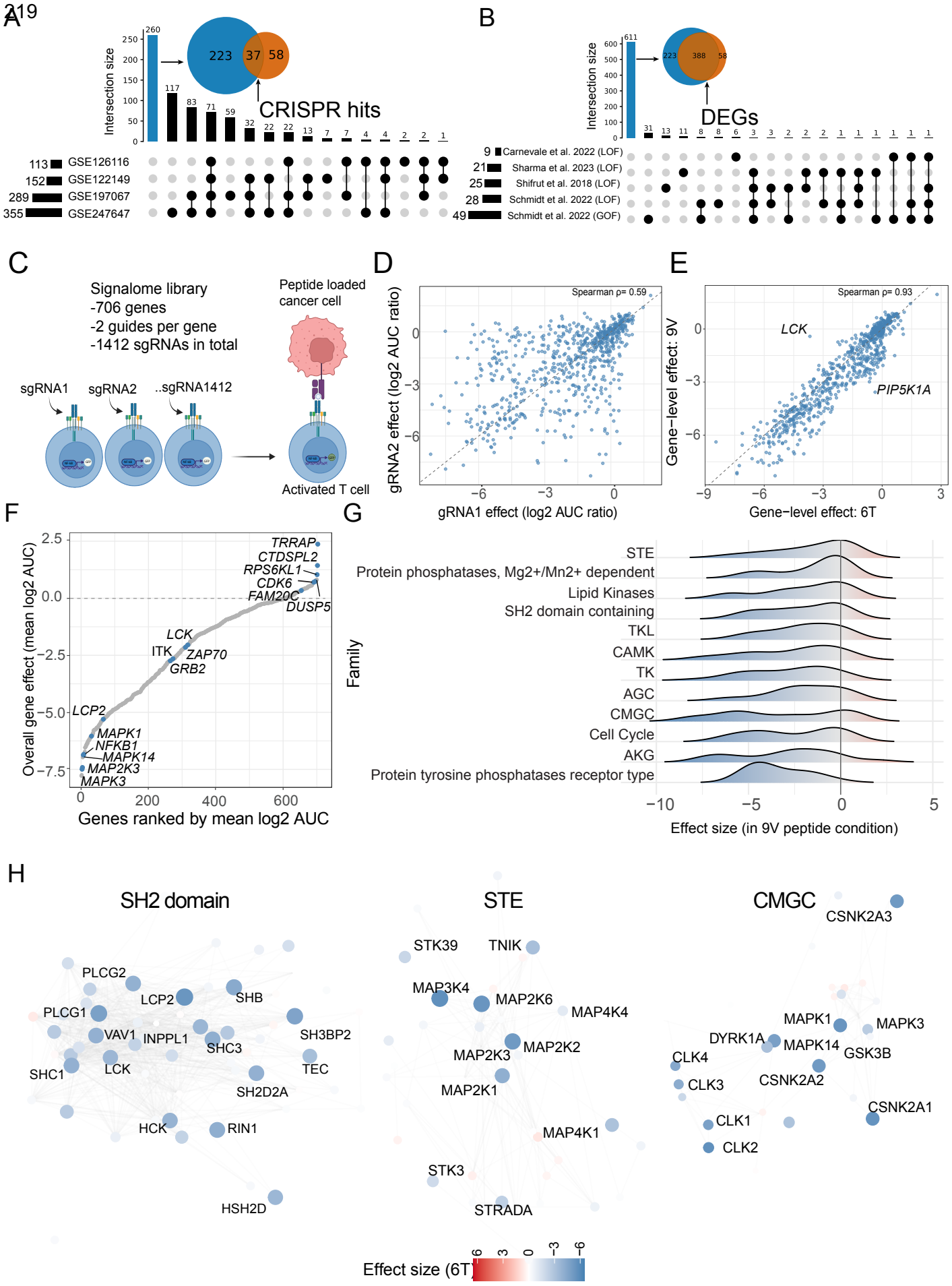
A
Intersection size
260
117
83
71
59
32
22
22
13
7
7
4
4
2
2
1
223
37
58
CRISPR hits
113 GSE126116
152 GSE122149
289 GSE197067
355 GSE247647
B
Intersection size
611
31
13
11
8
8
6
3
3
2
2
2
1
1
1
1
1
1
223
388
58
DEGs
9 Carnevale et al. 2022 (LOF)
21 Sharma et al. 2023 (LOF)
25 Shifrut et al. 2018 (LOF)
28 Schmidt et al. 2022 (LOF)
49 Schmidt et al. 2022 (GOF)
C
Signalome library
-706 genes
-2 guides per gene
-1412 sgRNAs in total
sgRNA1
sgRNA2
..sgRNA1412
Peptide loaded cancer cell
Activated T cell
D
Spearman ρ= 0.59
gRNA2 effect (log2 AUC ratio)
gRNA1 effect (log2 AUC ratio)
E
Spearman ρ= 0.93
LCK
PIP5K1A
Gene−level effect: 9V
Gene−level effect: 6T
F
Overall gene effect (mean log2 AUC)
Genes ranked by mean log2 AUC
TRRAP
CTDSPL2
RPS6KL1
CDK6
FAM20C
DUSP5
LCK
ITK
ZAP70
GRB2
LCP2
MAPK1
NFKB1
MAPK14
MAP2K3
MAPK3
G
Family
STE
Protein phosphatases, Mg2+/Mn2+ dependent
Lipid Kinases
SH2 domain containing
TKL
CAMK
TK
AGC
CMGC
Cell Cycle
AKG
Protein tyrosine phosphatases receptor type
Effect size (in 9V peptide condition)
H
SH2 domain
PLCG2
LCP2
SHB
PLCG1
VAV1
INPPL1
SHC3
SH3BP2
SHC1
LCK
TEC
SH2D2A
HCK
RIN1
HSH2D
STE
STK39
TNIK
MAP3K4
MAP2K6
MAP4K4
MAP2K3
MAP2K2
MAP2K1
MAP4K1
STK3
STRADA
CMGC
CSNK2A3
MAPK1
MAPK3
DYRK1A
MAPK14
GSK3B
CLK4
CSNK2A2
CLK3
CSNK2A1
CLK1
CLK2
Effect size (6T)

Figure 2: A signalome-wide, arrayed CRISPR perturbation screen reveals hierarchical and distributed control of NF-κB signalling in T cells. **A:** Overlap between genes that are not transcriptionally regulated across four T-cell–specific expression datasets and genes identified as hits in genome-wide CRISPR screens, revealing 37 signalling genes that are functionally required despite lacking dynamic expression changes. UpSet plot shows intersections across expression studies. **B:** Overlap between genes that are differentially expressed in at least one T-cell expression dataset and genes not identified as hits in genome-wide CRISPR screens, identifying 388 signalling genes that are transcriptionally regulated but not functionally required in pooled CRISPR screens. UpSet plot shows intersections across CRISPR studies. **C:** Schematic of the arrayed CRISPR perturbation strategy. **D:** Concordance between independent sgRNAs targeting the same gene under high-affinity stimulation (9V). Each point represents a gene; axes show $\log_2$(AUC ratio) for sgRNA1 versus sgRNA2. **D:** Comparison of gene-level perturbation effects between low-affinity (6T) and high-affinity (9V) stimulation conditions. Each point represents one gene collapsed across the two sgRNAs. **F.** Genes ranked by overall effect size, defined as the mean gene-level $\log_2$(AUC ratio) across both stimulation conditions. **G:** Distribution of effect sizes in 9V condition stratified by functional protein families **H:** Network representation of selected signalling modules with node colour indicating signed effect size under stimulation with low affinity antigen (6T). Nodes represent genes; edges correspond to curated functional interactions from STRING.

Targeted perturbation of SH2-domain-containing proteins in primary CD8$^+$ T cells validates functional TCR signalling dependencies

Although large-scale perturbation screens with functional read outs are readily implemented in cell lines, extending such approaches to primary human T cells remains challenging. To enable arrayed perturbation in primary CD8$^+$ T cells at scale, we established a workflow based on lentiviral delivery of sgRNAs followed by Cas9 electroporation, a strategy compatible with systematic perturbation, while avoiding the cost and scalability constraints of RNP-only approaches (*27*).

A further barrier to scalable functional assays in primary T cells is antigen specificity, as individual T cells respond only to their cognate TCR ligand. To circumvent this limitation, we employed bispecific molecules, which engage CD3 independently of endogenous TCR specificity (*32*, *33*). Here, the bispecific engager consists of an anti-CD3 single-chain variable fragment fused to a TCR targeting an HLA-A2-bound gp100 peptide (YLEPGPVTV), thereby

253 triggering TCR signalling and directing T-cell activation against gp100-pulsed A375 melanoma
254 cells (*18*). This approach enables the use of polyclonal primary $CD8^+$ T cells while preserving
255 physiologically relevant TCR-proximal signalling, thus substantially increasing experimental
256 scalability.

257 Upon co-culture with gp100-pulsed target cells, polyclonal $CD8^+$ T cells exhibited robust
258 upregulation of activation markers (CD69, CD25, 4-1BB) and potent cytotoxicity (**Fig. 3A**).
259 Despite these strong functional responses, phosphoprotein changes measured by CyTOF
260 remained limited (**Fig. 3B, Supplementary Figure 3**), consistent with the low signalling flux
261 observed during direct cell–cell interactions and reinforcing the sensitivity of functional
262 readouts for capturing signalling outcomes (*18*).

263 To validate the signalling architecture inferred from the Jurkat signalome screen in a
264 physiological setting, we focused on the SH2-domain-containing protein family, which
265 exhibited broad functional engagement in NF-κB regulation despite lacking a coherent pattern
266 of transcriptional regulation during T-cell activation (**Fig. 2G**). This family includes multiple
267 well-established TCR signalling components, making it a suitable test case for functional
268 validation. We targeted 66 SH2-domain-containing genes, along with control targets, in
269 polyclonal primary $CD8^+$ T cells from six independent donors using lentiviral sgRNA delivery
270 followed by Cas9 electroporation (**Supplementary Figure 4A**). Functional consequences
271 were assessed by quantifying target cell killing in co-culture assays (**Fig. 3C**).

272 Disruption of canonical TCR signalling components, including *LCK*, *LCP2*, and *ITK*, markedly
273 impaired $CD8^+$ T-cell cytotoxicity (**Fig. 3C,D**) and reduced expression of activation markers 4-
274 1BB (**Fig. 3E**) and CD25 (**Supplementary Figure 4B**) at 48 hours, validating the sensitivity
275 and specificity of the assay. After correcting for donor and batch effects (**Methods**), systematic
276 perturbation of the SH2 gene family revealed a spectrum of functional effects on cytotoxicity
277 **(Fig. 3F)**.

278 Genes were ranked by their impact on tumour cell killing, with cytotoxicity levels quantified
279 using the AUC metric (**Methods**). Our analysis revealed profiles that closely mirrored both
280 known TCR signalling annotations, and the dependencies observed in the Jurkat screen (**Fig.**
281 **3F**). Perturbation of key signalling mediators (*ITK*, *LCK*, *LCP2*, *PLCγ*, *PIK3R1-3*), adaptor
282 proteins (*GRAP*, *GRB2*), and cytoskeletal regulators (*VAV1*, *VAV3*) consistently reduced
283 $CD8^+$ T-cell cytotoxicity, whereas disruption of *SLA2* and *PTEN*, both known negative
284 regulator of TCR signalling, enhanced $CD8^+$ T-cell-mediated killing (**Fig. 3G; Supplementary**
285 **Fig. 4C,D**). These results demonstrate that the SH2 gene family constitutes a distributed and
286 functionally essential regulatory module in primary T-cell activation.

287 Because bispecific-based activation bypasses endogenous antigen specificity, we next asked
288 whether these dependencies were preserved in antigen-specific TCR-engineered T cells.
289 Primary $CD8^+$ T cells were transduced with plasmids encoding the 1G4-TCR and an LNGFR
290 tag, and TCR $V\beta13.1^+$ $LNGFR^+$ cells were sorted and expanded for use *in vitro*
291 (**Supplementary Fig. 4E**). This system enabled direct comparison of signalling requirements
292 across different ligand affinities. Consistent with the Jurkat screen, disruption of *LCK* exhibited
293 affinity-dependent effects: under high-affinity stimulation with the 3Y peptide, *LCK* targeting
294 had minimal impact on tumour cell killing, whereas under weaker stimulation conditions (6T),
295 cytotoxicity was strongly impaired (**Fig. 3G**).

296 Together, these results demonstrate that functional signalling dependencies identified in
297 Jurkat cells are largely conserved in primary human $CD8^+$ T cells. This validation establishes
298 the robustness of the perturbation-based framework across experimental systems and
299 highlights how distributed adaptor-mediated regulation and signal-strength–dependent
300 buffering shape TCR-driven functional responses.

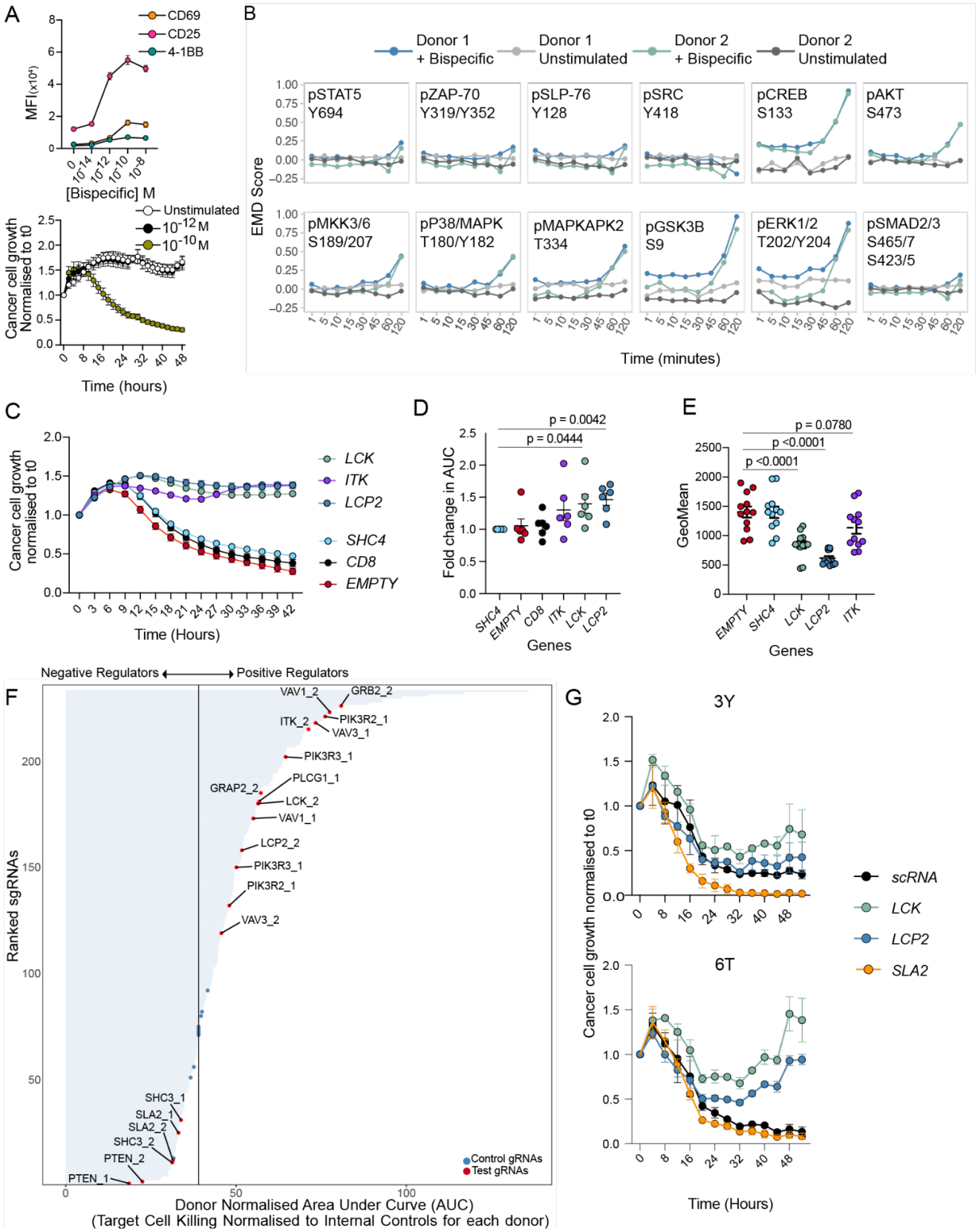

Figure 3: Targeted perturbation in primary CD8⁺ T-cells reveals the spectrum of activity of the SH2 gene family on T-cell cytotoxicity. A: Top panel - Expression (mean fluorescence intensity, MFI) of activation markers on CD8⁻ T-cells at 24 hours following co-

305 culture with gp100 pulsed A375 melanoma cell lines and a bispecific T cell engager. Bottom
306 panel - $CD8^+$ cytotoxic responses following co-culture with A375 melanoma cell lines as
307 described for the top panel. Data in both panels from 3 independent donors, representative of
308 at least 3 experimental repeats. **B:** Phosphorylation of early signalling mediators downstream
309 of TCR engagement as measured by mass cytometry (CyTOF). Data shown from two
310 independent donors in one experiment, representative of at least 4 independent donors across
311 4 experiments. **C:** Representative killing curves from $CD8^+$ T-cell co-cultures with A375
312 melanoma cells. T-cell activation was initiated through use of the bispecific engager at a final
313 concentration of 10^{-10}M. Targeting of known TCR-signalling mediators with sgRNAs inhibits
314 cytotoxic T-cell responses. Data show from one donor and one independent experiment,
315 representative of at least 6 independent donors across 6 independent experiments. **D:** Area
316 under the curve (AUC) analysis of killing curves shown in panel C, normalised to SHC4
317 targeted controls. Data from 6 independent donors across 6 independent experiments.
318 Statistical analysis performed by paired T-test. **E:** Targeting TCR-signalling mediators with
319 sgRNAs reduces surface 4-1BB expression, measured at 48 hours post co-culture with A375
320 melanoma cells as detailed in D. Data shown are the same T-cells from panel D, and are from
321 6 independent $CD8^+$ donors across 6 independent experiments. Statistical analysis performed
322 via One-Way ANOVA with Dunnett's multiple comparison tests. **F:** Waterfall plot of normalised
323 AUCs from killing curves illustrated in panel C, from experiments targeting all genes encoding
324 SH2-domain containing proteins. Killing curves for each perturbation were first normalised to
325 donor-specific internal negative control sgRNAs before computing AUC values. Ranked gene
326 analysis identifies both positive and negative regulators of T-cell cytotoxicity within the SH2
327 gene family. **G:** Representative killing curves from targeting *LCK*, *LCP2* or *SLA2* in primary
328 1G4-TCR^+ $CD8^+$ T-cells. A375 melanoma cell lines were pulsed with NY-ESO-1 peptides as
329 indicated to final concentrations of 100µg/mL. Data shown from one independent experiment,
330 representative of two independent repeats using two individual $CD8^+$ donors.

331 *TRRAP* and *CTDSPL2* constrain $CD8^+$ T-cell effector output downstream of TCR 332 signalling

333 Although the majority of perturbations in the signalome screen reduced NF-κB activity, a small
334 number of gene disruptions increased reporter output. Among these, targeting of *TRRAP* and
335 *CTDSPL2* consistently enhanced NF-κB-driven GFP expression in Jurkat cells (**Fig. 4A**).
336 TRRAP is a pseudokinase that functions as a scaffold within histone acetyltransferase
337 complexes involved in transcriptional regulation, whereas CTDSPL2 is a poorly characterized
338 serine/threonine phosphatase. Neither protein has been well defined in the context of T-cell
339 signalling, prompting further functional validation in primary cells.

340

341 To assess their roles in physiological settings, we targeted *TRRAP* or *CTDSPL2* in primary
342 human $CD8^+$ T cells using lentiviral sgRNA delivery followed by Cas9 electroporation.

343 Disruption of either gene significantly enhanced CD8$^+$ T-cell-mediated killing of A375
344 melanoma cells in bispecific-based co-culture assays (**Fig. 4B**). Consistent with increased
345 effector activity, targeting *TRRAP* or *CTDSPL2* also elevated IFNγ secretion at 24 hours (**Fig.**
346 **4C**). In addition, after targeting *TRRAP* or *CTDSPL2* we observed enhanced degranulation,
347 as measured by surface CD107α expression at 4 hours post A375 co-culture (**Fig. 4D**). These
348 results indicate that both proteins act to constrain T-cell effector responses downstream of
349 TCR-proximal signalling.
350
351 Because bispecific-based activation bypasses endogenous antigen specificity, we next
352 examined whether these effects were preserved in antigen-specific TCR-engineered T cells.
353 Primary CD8$^+$ T cells expressing the 1G4 TCR were electroporated with sgRNA–Cas9
354 ribonucleoprotein (RNP) complexes targeting *TRRAP* or *CTDSPL2*, and cytotoxic activity was
355 assessed against A375 melanoma cells presenting endogenous levels of NY-ESO-1.
356 Importantly, these experiments utilised a distinct, non-overlapping sgRNA sequence
357 compared to these utilised in our signalome-wide arrayed screen. Under these basal antigen
358 conditions, disruption of either gene significantly enhanced tumour cell killing relative to
359 scrambled controls (**Fig. 4E**). This enhancement was maintained across a range of peptide
360 affinities, again utilising 6T or 3Y NY-ESO-1 altered peptide ligands (**Supplementary Fig. 5A**).
361
362 Finally, to assess whether enhanced CD8$^+$ T-cell effector functions arising from *TRRAP* or
363 *CTDSPL2* perturbations were accompanied by an increase in markers of T-cell dysfunction
364 and exhaustion (e.g., PD-1, LAG-3 and TIM-3), cell surface expression of these molecules
365 was assessed in polyclonal CD8$^+$ T-cells 24 hours post stimulation with A375 melanoma cells
366 and the bispecific engager. Phenotypically, *TRRAP* or *CTSPL2* targeted T-cells were similar
367 to the unedited, empty plasmid controls, where expression of these three inhibitory receptors
368 displayed an activation-marker-like expression pattern. Expression of surface PD-1, LAG-3
369 and TIM-3 all correlated with the bispecific concentration utilised to initiate T-cell activation in

370 these experiments, and reduced expression was observed in the *LCP2* targeted control
371 (**Supplementary Fig. 5B**).

372 To investigate how TRRAP and CTDSPL2 depletion enhanced cytotoxicity, we performed
373 RNA sequencing following CRISPR-mediated perturbation in primary $CD8^+$ T-cells. TRRAP is
374 a scaffold component of the SAGA and TIP60 histone acetyltransferase complexes and
375 supports MYC- and E2F-dependent transcriptional programs. Consistent with this role, upon
376 activation, TRRAP-deficient T cells exhibited coordinated downregulation of genes associated
377 with cell cycle progression and DNA replication, including CENPA, PLK1, POLE2, and multiple
378 MCM complex components. In contrast, inflammatory and immune signalling genes, including
379 IFITM5, IL23R and NR4A family components were upregulated (**Figure 4F, Supplementary**
380 **Table 4**). Pathway-level analysis revealed suppression of proliferative programs alongside
381 enrichment of inflammatory and cytokine signalling modules (**Figure 4G**). These findings
382 suggest that TRRAP loss shifts T cells away from a proliferative transcriptional state toward
383 an inflammatory, effector-associated profile. By contrast, CTDSPL2-deficient cells displayed
384 minimal global transcriptional remodelling. Donor-paired analyses demonstrated that most
385 genes remained near baseline at both stimulated and unstimulated conditions
386 (**Supplementary Fig. 5C, Supplementary Table 4**). The increased killing arising from
387 *CTDSPL2* perturbation is, therefore, unlikely to arise from large-scale transcriptional
388 reprogramming and instead reflects altered signalling dynamics.

389 Together, these data identify TRRAP and CTDSPL2 as previously unrecognized negative
390 regulators of $CD8^+$ T cell effector function. Their disruption enhances cytotoxicity, cytokine
391 production, and degranulation under both polyclonal and antigen-specific activation conditions
392 without inducing excessive expression of inhibitory receptors. These findings highlight novel
393 regulatory nodes that may be therapeutically leveraged to enhance T cell–based
394 immunotherapies.

395

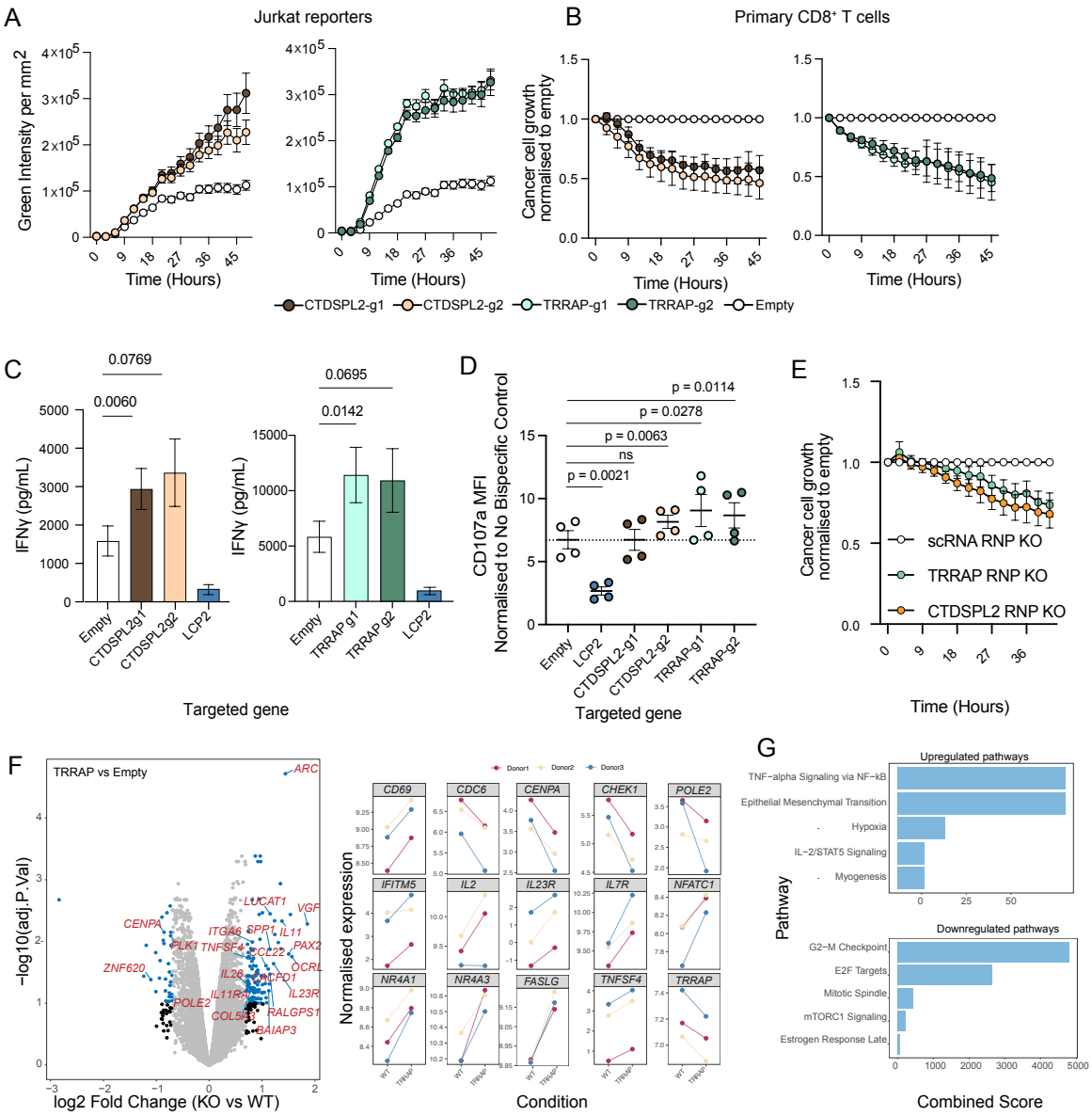

Figure 4: Perturbation of novel targets *CTDSPL2* and *TRRAP* enhances primary CD8⁺ T-cell functional activity. A: NFkB-GFP traces from 1G4-TCR⁺ Jurkat reporters when transduced with *CTDSPL2* (left) or *TRRAP* targeting sgRNAs (right). Jurkat cells were stimulated with A375 melanoma cell lines pulsed with NY-ESO-1 9V peptide (100µg/mL). **B:** Cytotoxic responses from primary CD8⁺ T-cells when co-cultured with A375 melanoma cell lines pulsed with gp100 peptide and a bispecific T-cell engager (final concentration 10^{-11}M). Data shown from 9 independent donors across 3 experiments (TRRAP sgRNAs) or a minimum of 4 independent donors across 2 experiments (CTDSPL2 sgRNAs). A375 cell growth was normalised to the empty control for each donor. **C:** IFN_{γ} secretion at 24 hours from primary CD8⁺ T-cells stimulated as described for panel B. Data shown from 2 independent donors across 1 individual experiment, representative of at least 4 independent donors across 2 experiments. Statistical analysis performed via One-Way ANOVA with Dunnett's multiple comparisons. **D:** CD107α mean fluorescence intensity (MFI) from CD8⁺ T-cells stimulated as described for panel B, measured at 4 hours post stimulation. CD107a expression was normalised to unstimulated controls (no bispecific) for each CRISPR targeting condition. Data

shown from 4 independent donors across 2 experiments. **E:** Cytotoxic responses of 1G4-TCR$^+$ primary CD8$^+$ T-cells when co-cultured with A375 melanoma cell lines expressing basal NY-ESO-1. 1G4-TCR$^+$ CD8$^+$ T-cells were electroporated with RNPs targeting either *CTDSPL2* or *TRRAP*, together with a scrambled control (scRNA). Data shown from 6 donors across 3 independent experiments. Growth curves were normalised to the scRNA controls for all donors. **F.** Differential gene expression analysis of *TRRAP*-targeted primary CD8$^+$ T cells following stimulation. Volcano plot showing $\log_2$ fold change (KO vs WT) versus $-\log_{10}$ adjusted P value from donor-controlled limma-voom analysis (n = 3 donors). Selected representative genes are highlighted. Inset panels show donor-resolved normalized expression for representative upregulated inflammatory genes (e.g., IL2, IL7R, IL23R, TNFSF4) and downregulated proliferative genes (e.g., CDC6, CENPA, CHEK1, POLE2). Lines connect paired donor samples. TRRAP transcript abundance was modestly but consistently reduced across donors (see Fig. 4F, inset). **G**. Pathway enrichment analysis of differentially expressed genes in *TRRAP*-targeted cells. Hallmark gene set enrichment (Enrichr) identified suppression of proliferative programs, including G2/M checkpoint and E2F target pathways, and enrichment of inflammatory and TNFα–NF-κB signalling modules. Combined enrichment scores are shown.

Discussion

In this study, we present a perturbation-based framework to interrogate cellular signalling during physiological cell–cell engagement. Leveraging functional readouts rather than direct measurement of signalling intermediates allowed us to identify key signalling regulators despite remarkably low signalling flux under these conditions (*18*). By quantifying transcription factor activity following systematic perturbation of signalling components, we could capture pathway activity through integrated transcriptional outputs rather than discrete molecular states. This approach is motivated by models of temporal signal integration, as articulated by Purvis and Lahav, and by subsequent optogenetic studies demonstrating that many proximal T-cell signalling intermediates decay rapidly following receptor disengagement (*34*, *35*). In contrast, transcriptional outputs integrate signalling over time, accumulating to provide a longer-lived functional record of signalling activity. In the context of T-cell activation, our findings support this framework by demonstrating that robust NF-κB activation and effector responses results from low-amplitude or spatially restricted signalling during direct T-cell-tumour cell engagement.

444 A key feature of this framework is its compatibility with physiologically relevant stimulation
445 formats. By interrogating signalling in cell–cell co-culture systems, our approach avoids
446 reliance on supraphysiological stimulation commonly required to elicit detectable changes in
447 phosphorylation or kinase activity, and instead captures the integration of complex signal
448 inputs that arise during direct cellular interactions. Although strong stimulation (most often
449 achieved using anti-CD3/CD28 bead-based activation) has been instrumental for defining
450 canonical signalling pathways in global phosphoproteomic studies (*3*, *5*, *11*), it may not reflect
451 signalling behaviour in physiological settings. This limitation is particularly relevant in studies
452 of T-cell activation, where signalling outcomes reflect the combined influence of antigen
453 affinity, co-stimulatory, and inhibitory inputs, such that maximal pathway activation cannot be
454 assumed to be an appropriate starting point for interrogating authentic signalling processes.
455 Similar considerations apply to high-dimensional single-cell approaches, including mass
456 cytometry, which have provided powerful insights when phosphorylation flux is sufficiently
457 robust, but which typically rely on maximal signalling to infer signalling relationships (*17*, *36*).

458 Applying this strategy to T-cell receptor signalling revealed that the nodes important for
459 functional signalling are largely unchanged at different stimulation strengths produced by
460 differing-quality TCR ligands, whereas there do exist specific nodes that are highly context
461 dependent. Perturbation of *LCK*, a widely studied SRC-kinase which is known to initiate
462 receptor signalling from the TCR (31) exhibited a strong dependence on ligand affinity;
463 disruption of both markedly impaired NF-κB activation under weak stimulation but was
464 buffered under high-intensity conditions. Quantitative modulation of proximal kinase activity
465 has been described for LCK. Partial reduction of LCK activity preferentially impairs T cell
466 responses to low-affinity or low-dose antigen, whereas strong stimulation can partially
467 compensate for diminished kinase availability (*30*, *37*, *38*). Notably, Cabezas-Caballero and
468 colleagues demonstrated that altering coreceptor identity (swapping CD8 and CD4) effectively
469 redistributes and sequesters LCK, thereby tuning TCR sensitivity by modulating the local
470 availability of active kinase. This work highlights how LCK availability functions as a

quantitative regulator of signalling output. Together, these findings outline how targeting key proximal signalling components can serve as a mechanism to engineer tuning of cellular signalling in the context of varied stimulation strengths.

Beyond individual nodes, our data reveal how signalling control is unequally distributed across molecular families. Rather than treating pathway components as interchangeable, our perturbation-based analysis quantifies family-level engagement, distinguishing signalling nodes dominated by a small number of high-impact components from those that rely on distributed contributions. This is exemplified by the MAPK pathway, in which NF-κB regulation was driven primarily by a limited set of kinases, consistent with bottlenecked enzymatic cascades. In contrast, SH2-domain–containing proteins exhibited broad functional engagement, reflecting their role as proximal adaptors that integrate receptor-derived signals and connect them to diverse downstream pathways. These patterns are consistent with the early proposal by Pawson and colleagues, i.e., that signalling networks are assembled from conserved interaction modules whose combinatorial deployment confers specificity, robustness, and evolutionary adaptability without reliance on rigid, linear pathways (*39–41*). Our inferred signalling network therefore supports a modular, hierarchical organisation in which control is unevenly distributed across molecular layers and funnelled through preferred pathways under defined conditions.

Notably, many SH2-domain-containing proteins exerted strong functional effects despite limited transcriptional regulation across T-cell activation states. This suggests that signalling control at this level operates largely through constitutively expressed components whose regulatory capacity is governed post-translationally, through phosphorylation, conformational changes, and dynamic recruitment to signalling complexes. As a result, expression-based analyses may underestimate this contribution to signalling control, whereas perturbation-based functional approaches are particularly well suited to reveal their role.

496 Finally, our experimental framework enabled the identification of previously unrecognised
497 negative regulators of T cell effector function, specifically TRRAP and CTDSPL2. TRRAP
498 functions as a core scaffold for multiple histone acetyltransferase complexes, thereby
499 regulating chromatin accessibility and transcriptional output downstream of diverse signalling
500 pathways (*42*). Consistent with this role, TRRAP depletion resulted in coordinated suppression
501 of proliferative and DNA replication–associated transcriptional programs alongside enrichment
502 of inflammatory and immune signalling modules, indicating a redistribution of transcriptional
503 state rather than global activation. In contrast, CTDSPL2 is a poorly characterised
504 serine/threonine phosphatase implicated in transcriptional regulation and cell-state control,
505 and its role in T cell biology has not previously been examined (*43*). Notably, CTDSPL2
506 depletion enhanced cytotoxicity with minimal global transcriptional remodelling, suggesting
507 that its effects are mediated primarily through altered signalling dynamics rather than broad
508 transcriptional reprogramming. These findings provide functional validation of nodes identified
509 in the signalome-wide arrayed perturbation screen and illustrate how this approach can
510 uncover regulatory layers that modulate signalling output and effector potential that may be
511 overlooked by pooled genetic screens.

512 In conclusion, whereas genome-wide perturbation screens and high intensity stimulation-
513 based approaches have been effective for defining essential signalling components, they are
514 less well-suited to dissecting signalling networks dependent on quantitative effects. By
515 emphasising quantitative, time-resolved functional outputs in the setting of physiological
516 stimulation, the framework presented here offers a general strategy for interrogating cell
517 responses as the field moves toward a system-level understanding of signalling.

518 # Materials and Methods

519 ## Cell culture

520 All Jurkat cell lines were cultured in RPMI-1640 medium (Gibco, #21875-034) supplemented
521 with 10% FCS (Gibco, #A5256801, Lot #B3024242RP), 1% Penicillin-Streptomycin-Neomycin
522 (Sigma-Aldrich, #P4083), 1% L-Glutamine (Sigma-Aldrich, #G7513), 1% Sodium Pyruvate
523 (Sigma-Aldrich, #S8636) and 1% HEPES (Gibco, #15630-056). HEK293-T cells for lentivirus
524 production were cultured in DMEM complete medium (Gibco, #41965-039) supplemented as
525 described for the RPMI-1640 Jurkat medium. A375 melanoma cell lines were cultured in
526 DMEM-F12 medium (Gibco, #11320-033) supplemented with 10% FCS, 1% Penicillin-
527 Streptomycin-Neomycin, 1% Sodium Pyruvate and 1% HEPES. Finally, all primary human
528 cells were cultured in RPMI-1640 medium supplemented with 10% human serum, 1%
529 Penicillin-Streptomycin-Neomycin, 1% L-Glutamine, 1% Sodium Pyruvate, 1% non-essential
530 amino acids (NEAA, Gibco, #11140), 1% HEPES and 0.1% B-mercaptoethanol (Gibco,
531 #31350-010).

532 ## Production of 1G4^{+} Jurkat NF-kB GFP reporter cell lines

533 Jurkat T-cells (ATCC) were first transduced with the Cas9 encoding plasmid pKLV2-EF1a-
534 Cas9Bsd-W, as previously described (*26*), to produce Cas9 expressing Jurkat cell lines. Next,
535 Cas9^{+} Jurkat cells were transduced with pSIRV-NF-kB-eGFP construct which was a gift from
536 Peter Steinberger (Addgene plasmid # 118093)(*44*) prior to single cell cloning and selection
537 of NF-kB GFP expressing clones. Endogenous TCR was then deleted from these lines via
538 electroporation with a TRAC/TRBC sgRNA - Cas9 RNP complex. For the generation of RNPs,
539 sgRNAs targeting TRAC and TRBC1/2 (IDT, TRAC sequence:
540 AGAGTCTCTCAGCTGGTACA, TRBC1/2 sequence: GGAGAATGACGAGTGGACCC) (*45*)
541 was pre-incubated with Cas9 (IDT, #10007807) at room temperature for 30 minutes. Here,
542 0.73µL of each sgRNA (400µM) was added to 0.5µL of Cas9 (62µM). Electroporation was

543 then performed using the Lonza P3 Nucleofector kit (Lonza, # V4SP-3096) as per
544 manufacturer's instructions. Briefly, one million Jurkat cells were resuspended in 20µL P3
545 buffer (Lonza, #V4SP-3096), to which the complexed RNP was added. Cells were then moved
546 to one well of a 16-well electroporation strip for electroporation with a Lonza Nucleofector on
547 programme #E0115. Cells were immediately recovered from the electroporation strip by the
548 addition of 80µL of media before returning them to culture. Following deletion of endogenous
549 TCR, Cas9^{+} NF-kB GFP^{+} TCR$^{-/-}$ Jurkats were then transduced with constructs encoding for
550 the 1G4-TCR (*18*) to produce the final 1G4^{+} Cas9^{+} NF-kB GFP^{+} Jurkat cell lines.

551 sgRNA design and cloning

552 To design sgRNA molecules, the top two candidates from CRISPick (Broad Institute) were
553 selected for each gene. sgRNA sequences were purchased as oligos in both forward and
554 reverse orientations (Sigma-Aldrich) prior to annealing, and were then cloned into the BbsI
555 site of the CRISPR sgRNA expression vector pKLV2-U6gRNA5(BbsI)-PGKpuro2ABFPW
556 (Addgene, #67974) as previously described (*46*). All sgRNA sequences produced for the
557 signalome library are displayed in supplementary table 1.

558 Lentivirus production

559 Lentiviruses were prepared by transfecting HEK293T with the sgRNA expression vector.
560 Firstly, 500ng sgRNA expression plasmid was combined with 250ng pMD2.G (Addgene,
561 #12259) and 1.2µg psPAX.2 (Addgene, #12260) in 500µL optiMEM (Gibco, #13985062). To
562 this, 2µL plus reagent (Thermo Fisher, #15338100) was added prior to mixing by inversion
563 and incubation at room temperature for 5 minutes. Next, 6µL lipofectamine-LTX (Thermo
564 Fisher #15338100) was added and the solution was again inverted to mix, prior to incubation
565 at room temperature for 30 minutes. This optiMEM mixture was then added to HEK293T cells
566 in a 6 well plate together with 2mL of DMEM medium supplemented as described above.
567 Lentiviral supernatants were then harvested at 48-72hrs and filtered through a 0.45µm filter.

568 All lentiviruses were either used immediately or stored at -80°C until use, but were never
569 freeze-thawed.

570 Peptide sequences for A375 pulsing

571 Where indicated, A375 melanoma cell lines were pulsed with the following NY-ESO-1
572 altered peptide ligands to induce TCR signalling downstream of the 1G4-TCR. Peptide
573 pulsed A375 cell lines were co-cultured with either Jurkat or primary $CD8^+$ T-cells as
574 indicated, and final peptide concentrations are shown throughout the text. All peptides were
575 ordered from Genscript with a purity >95% and were reconstituted in DMSO upon arrival,
576 stored at -80°C, and never freeze-thawed more than twice. 9V: SLLMWITQV, 3Y:
577 SLYMWITQV, 3I: SLIMWITQV, 6T: SLLMWTTQV. Affinities (K_D) for these NY-ESO-1
578 peptides have been previously described (9V ≅ 7.2μM, 3Y ≅ 30μM, 3I ≅17μM, 6T ≅ 101μM)
579 (*47*). Finally, for experiments utilising bispecific T-cell engagers, A375 cell lines were pulsed
580 with the gp100 peptide (10μg/mL, sequence: YLEPGPVTV) as described, which was also
581 obtained from Genscript at >95% and handled as per the NY-ESO-1 altered peptide ligands.

582 Arrayed screening of the signalome in 1G4-TCR^+ Jurkat reporter cell lines

583 $1x10^5$ 1G4-TCR^+ Jurkat NF-kB GFP reporter cells were transduced with 100μL of the arrayed
584 library lentivirus in a 96-U bottomed plate, in a total of 200μL. Transduction was performed by
585 centrifugation at 800g, 90min, 32°C. After 48hrs, transduced cells were grown in the presence
586 of puromycin (1μg/mL final concentration, Gibco, #A11138-03) to select only transduced cells.
587 At day 7, transduced Jurkat reporter cells were counted via flow cytometry alongside
588 simultaneously ensuring transduction and selection success via expression of the BFP tag in
589 the sgRNA plasmid. All cells were 95-100% BFP^+. Following this counting, all culture volumes
590 across the arrayed library were normalised to allow for consistent cell numbers to be utilised
591 in co-cultures with A375 melanoma cells. Here, A375 melanoma cells were treated with

592 100µg/mL of 6T or 9V NY-ESO-1 peptides (alongside a no peptide control), before plating
593 5,000 cells in 25µL in a 384 well plate (Falcon, #353961), to which 10,000 Jurkat reporter cells
594 were added in 25µL. NF-kB signalling pathway activation downstream of TCR engagement
595 was measured using IncuCyte imaging for 42-48 hours.

596 Arrayed screen analysis in Jurkat cells

597 Raw IncuCyte time-course data from multiple experiments and plates were aggregated and
598 annotated with experimental metadata. Condition labels were harmonized, and control wells
599 were explicitly annotated. For each peptide, signalling output was summarized by calculating
600 the area under the curve (AUC) using trapezoidal integration. Data was collected for a total of
601 706 genes with signalome library. AUC values were normalized within each experiment and
602 condition to the median AUC of empty control wells and log2-transformed for downstream
603 analysis.
604
605 Each gene was targeted by two independent gRNAs. Guide-level effects were computed as
606 mean log2-normalized AUC ratios across replicates. Gene-level effects were derived using a
607 rule-based guide collapsing strategy that accounts for guide concordance and effect strength.
608 When guide effects were concordant (AUC within 1), their median was used; in cases of strong
609 discordance (particularly when one guide showed a weak effect or when guides had opposite
610 signs) the guide with the larger absolute effect was retained. Guide concordance was
611 assessed using Spearman correlation and same-direction agreement.
612
613 Gene-level effects were computed independently for each stimulation condition (6T and 9V)
614 and compared using Spearman correlation. A composite discordance score integrating effect
615 size differences and sign reversals was used to prioritize condition-specific dependencies.
616 Genes were annotated with functional families and essentiality, and family-level effect
617 distributions were visualized to identify pathway-level trends.

618 ## Primary CD8$^+$ T-cell transduction

619 Primary CD8$^+$ T-cells were isolated from healthy donor leukocyte cones obtained from the
620 NHS blood-transfusion service. CD8$^+$ T-cells were isolated using RosetteSep human CD8$^+$ T-
621 cell enrichment cocktail (StemCell, #15023) as per manufacturer's instructions. Isolated CD8$^+$
622 T-cells were then stimulated for 48 hours prior to transduction with 10µL/mL of CD3/CD28
623 immunocult (StemCell, #10971) and 50U/mL IL-2 (Biolegend, #589104), with cells at 2x10^6/mL
624 and 2mL/well in a 48 well plate. 250µL of Retronectin solution (Takara Bio, #351178) at
625 25µg/mL was added to non-treated 24-well tissue culture plates (Costar, #3738) for 24 hours
626 at 4°C prior to transduction. On the day of transduction, Retronectin solution was removed
627 and plates were blocked by addition of 300µL of 2% BSA in PBS (w/v) for 30 minutes at room
628 temperature. The BSA solution was then removed and wells were washed once in 500µL PBS,
629 before addition of 1.5mL of lentiviral supernatant and centrifugation at 2000g for 90 minutes,
630 32°C, no brake. Following centrifugation, all lentiviral supernatant (except 200-250µL to
631 prevent the well from drying) was removed from the well and 10^6 CD8$^+$ T-cells were seeded
632 into the well in 1mL of complete RPMI with supplementation of IL-2 at 50U/mL. Cells were
633 briefly spun onto the lentiviral coated wells at 2000rpm for 2 minutes, 32°C with the brake
634 applied. Transduction efficiency was assessed 48-72 hours post transduction by measuring
635 BFP expression via flow cytometry. Transduced cells were then selected by the addition of
636 puromycin to 1µg/mL (Gibco, #A11138-03), prior to electroporation with Cas9 protein.

637 ## Electroporation of primary CD8$^+$ T-cells

638 Transduced primary CD8$^+$ T-cells were electroporated with Cas9 protein (IDT, #10007807)
639 once BFP expression had reached >75-80%. Electroporation was performed using the Lonza
640 P3 Primary cell nucleofection kit (Lonza, #V4SP-3096) as per manufacturer’s instructions.
641 Here, 10^6 CD8$^+$ T-cells were resuspended in 20µL P3 buffer (Lonza, #V4SP-3096), to which
642 0.5µL Cas9 (62µM stock) was added. CD8$^+$ T-cells were then transferred to 1 well of the 16-
643 well electroporation strip before electroporation on programme #E0115. Immediately after

644 electroporation, cells were recovered by the addition of 80µL of complete RPMI-1640 medium
645 supplemented with 50U/mL IL-2. Cells were then plated across 2 wells in a 96 well-flat
646 bottomed tissue culture plate, each in 200µL with IL-2 at 50U/mL. Cells were maintained at 1-
647 $2x10^6$/mL, in the presence of 50U/mL IL-2 and 1µg/mL puromycin, until day 7 post
648 electroporation at which point functional assays were performed. All sgRNA sequences used
649 in the signalome library are displayed in supplementary table 1. Where indicated, perturbations
650 were also performed with RNPs, using independent and non-overlapping guides (IDT) from
651 the signalome library. Guide sequences used for RNP based perturbations are as follows:
652 TRRAP: AGTGGTCTGGTCAACCACCG, CTDSPL2: TTATTCATCAGCCCACGCGG, LCK:
653 GACCCACTGGTTACCTACGA, LCP2: TGAAGAAGTACCACATCGAT, SLA2:
654 GGGACCGGATCAGACACTAC, scRNA: GTATTACTGATATTGGTGGG.

655 A375 melanoma cytotoxicity and T-cell degranulation assays

656 At day 7 post Cas9 electroporation, $5x10^4$ A375 mOrange$^+$ melanoma cells were plated in
657 100µL in a 96 well-flat bottomed tissue culture plate and pulsed with gp100 peptide at a final
658 concentration of 10µg/mL. Cells were incubated at 37°C for at least 4 hours to allow for cell
659 adherence and antigen presentation. A375 cells were then washed once in PBS before
660 addition of $1x10^5$ CD8$^+$ T-cells in 100µL, and 100µL of the gp100-HLA-A2 - CD3 bispecific
661 engager to final concentrations as indicated. Details of this bispecific T-cell engager have been
662 previously described (*18*). Growth of the A375 melanoma cell line was then tracked for
663 approximately 48 hours via IncuCyte imaging, tracking the A375-expressed mOrange
664 fluorescent protein, allowing for quantification of T-cell mediated cytotoxicity (*26*). CD8$^+$ T-cell
665 degranulation was assessed at 4 hours post co-culture by flow cytometry with staining with
666 the following antibodies: CD8 PeCy7, 1:200, Biolegend #344712, CD107α PE, 1:500,
667 Biolegend #328608 and eBioscience fixable viability dye 780, 1:1000, Thermo Fisher #65-
668 0865-18.

669 ## RNA sequencing in primary CD8$^+$ T-cells

670 To assess transcriptional changes with *TRRAP* perturbation, we first targeted *TRRAP* via
671 lentiviral delivery of sgRNA and electroporation of Cas9 protein as previously described. For
672 these experiments, three primary CD8$^+$ T-cell donors were transduced with lentiviruses
673 encoding the TRRAPg1 sequence, or empty plasmid controls. On day 7 post Cas9
674 electroporation, 5x10^5 CD8$^+$ T-cells were activated on OKT3 coated 48-well tissue culture
675 plates for 3 hours. OKT3-coated tissue culture plates were prepared in advance, where each
676 well was treated with 300µL of Ultra-LEAF OKT3 at 1µg/mL (Biolegend, #317326), or PBS
677 only for unstimulated controls. After 3 hours, cells were recovered, washed in PBS and RNA
678 was extracted using the Qiagen RNA mini kit (#74104) as per manufacturer's instructions.
679 Isolated RNA was then sent to Novogene for NGS. FASTQ files were aligned using STAR
680 version 2.7.3a and quantified using featureCounts version 2.0.6. Ensembl Homo sapiens
681 GRCh38.86 was used as the reference genome. Lowly expressed genes were filtered out,
682 and gene expression distributions of each sample were normalised using edgeR version
683 3.42.2. Differential expression analysis was performed using limma version 3.54.2.
684
685 For experiments investigating transcriptional changes associated with *CTDSPL2*
686 perturbation, primary CD8$^+$ T-cells from two donors were transduced with lentiviruses
687 encoding for the CTDPSL2g1 or CTDSPL2g2 sequences, alongside empty plasmid controls.
688 Again, at day 7 post Cas9 electroporation, T-cells were stimulated as described as per
689 *TRRAP* perturbations. At 3 hours post stimulation on plate-bound OKT3, T-cells were
690 collected and resuspended in 50µL DNA/RNA shield (Zymo Research, #R1100-250) and
691 sent to Plasmidsaurus for NGS. Data handling and analysis was performed by
692 Plasmidsaurus as follows: Quality of the fastq files was assessed using FastQC v0.12.1.
693 Reads were then quality filtered using fastp v0.24.0 with poly-X-tail trimming, 3' quality-
694 based tail trimming, a minimum Phred quality score of 15, and a minimum length
695 requirement of 50bp. Quality-filtered reads were aligned to the reference genome using

696 STAR aligner v2.7.11 with non-canonical splice junction removal and output of unmapped
697 reads, followed by coordinate sorting using samtools v1.22.1. PCR and optical duplicates
698 were removed using UMI-based deduplication with UMIcollapse v1.1.0. Alignment quality
699 metrics, strand specificity, and read distribution across genomic features were assessed
700 using RSeQC v5.0.4 and Qualimap v2.3, with results aggregated into a comprehensive
701 quality control report using MultiQC v1.32. Gene-level expression quantification was
702 performed using featureCounts (subread package v2.1.1) with strand specific-counting,
703 multi-mapping read fractional assignment, exons and three prime UTR as the feature
704 identifiers, and grouped by gene_id. Final gene counts were annotated with gene biotype
705 and other metadata extracted from the reference GTF file.

706 Flow cytometry for assessment of $CD8^+$ T-cell phenotype

707 Genetically perturbed $CD8^+$ T-cells were stimulated on gp100 pulsed A375 melanoma cell
708 lines together with the bispecific T-cell engager as described. At 24 hours post stimulation,
709 T-cells were recovered and transferred to a 96-U bottomed plate before staining with 100µL
710 of antibody mix containing the following antibodies, all used at 1:200 unless otherwise
711 stated: CD8 PE-Cy7, Biolegend, #344750, PD-1 Alexa Fluor 647, Biolegend, #329910,
712 LAG3 FITC, Biolegend, #369308, TIM-3 PE, Biolegend, #345006, 4-1BB BV711, Biolegend,
713 #309832, and eBioscience fixable viability dye 780, 1:1000, Thermo Fisher, #65-0865-18.
714 Surface staining was performed at 4°C for a minimum of 20 minutes, before cells were
715 washed twice and acquired on a BD-LSR Fortessa. Data were then analysed in FlowJo
716 (version 10).

717 CRISPR-Cas9 mediated targeting of the SH2 domain gene family in 718 primary $CD8^+$ T-cells

719 Primary $CD8^+$ T-cells were isolated from healthy donor leukocyte cones and transduced with
720 lentiviruses encoding sgRNA molecules targeting all SH2 domain containing genes as

721 previously described (**Supplementary Table 1**). Due to the size of this family, this analysis
722 was split across 6 independent healthy $CD8^+$ T-cell donors, where each donor was
723 consistently assayed against an internal control sgRNA panel consisting of guides targeting:
724 *LCK*, *LCP2*, *ITK*, *CD8* and *SHC4* together with an empty plasmid control. Following
725 electroporation of Cas9 to induce perturbation of these genes, $CD8^+$ T-cells were co-cultured
726 with gp100 pulsed A375 melanoma cell lines, and the bispecific T-cell engager to a final
727 concentration of 10^{-10}M. Cytotoxic responses of $CD8^+$ T-cells were assessed by measuring
728 A375 melanoma growth, for a period of 48 hours. After 48 hours, $CD8^+$ T-cells were
729 harvested and stained with the following antibody cocktail at 4°C for 20 minutes to assess
730 activation marker expression (CD8 PeCy7, 1:200, Biolegend #344712; CD25 AF647, 1:200,
731 Biolegend #302618; 4-1BB BV711, 1:200, Biolegend #309832; eBioscience fixable viability
732 dye 780, 1:1000, Thermo Fisher #65-0865-18).

733 Donor-donor normalisations in primary $CD8^+$ T-cell killing assays
734 targeting SH2 domain family genes

735 In order to account for differing cytotoxic capacities between all $CD8^+$ T-cell donors used to
736 cover perturbation of the entire SH2 domain gene family, killing curves for each perturbation
737 were first normalised to their corresponding internal negative control for each individual
738 donor. This allows for the effect of targeting any given gene within the family to be compared
739 with other genes in the family that were assayed on separate donors, given the size of the
740 SH2 family. Next, to produce a single quantitative parameter for each gene, the area under
741 the curve (AUC) was calculated for all normalised killing curves using the trapz function from
742 the pracma package in R-studio (version 2024.09.1)(*48*). This analysis produced an
743 individual value for targeting each gene within the family, which was used to determine
744 whether this gene behaved as a negative or positive regulator of $CD8^+$ T-cell responses (**Fig
745 3F**).

746 ## Production of primary CD8$^+$ 1G4-TCR$^+$ T-cells and subsequent
747 cytotoxicity assays

748 CD8$^+$ T-cells isolated from healthy donor leukocyte cones were lentivirally transduced with
749 plasmid encoding for the 1G4-TCR together with a LNGFR tag as previously described (*18*).
750 Next, cells were then stained with TCR Vβ13.1 APC (Biolegend, #362408) and LNGFR FITC
751 (Miltenyi Biotech, #130-113-423) at 1:200 and double positive events were purified by
752 fluorescence-activated cell sorting. At the same time, PBMCs were isolated from three
753 separate healthy donor leukocyte cones, and were subjected to an irradiation dose of 3000rad.
754 Irradiated PBMCs were then centrifuged at 300g for 5 minutes, and resuspended at 2x10^6/mL
755 in complete RPMI-1640 medium. Equal volumes of PBMCs from each of the three donors was
756 then combined, before supplementation of the mixture with 200U/mL IL-2, 1X PHA (500X
757 stock, Invitrogen, #00-4977-03) and 50ng/mL OKT3 (Biolegend, #), to produce T-cell rapid
758 expansion medium (REM). Approximately 1x10^5 sorted LNGFR$^+$ TCR Vβ13.1$^+$ CD8$^+$ T-cells
759 was then added to 10mL REM and cultured for 5 days before counting and re-seeding to 10^6
760 cells/mL in complete RPMI-1640 medium with 200U/mL IL-2. Cells were then expanded for a
761 further 10-12 days, maintaining IL-2 concentrations at 200U/mL and cell densities at 1-
762 2x10^6/mL throughout. Resultant CD8$^+$ T-cell cultures were checked for purity via flow
763 cytometry and staining with CD8 PeCy7, TCR Vβ13.1 APC and LNGFR FITC. Functional
764 reactivity was then assessed by co-culture with NY-ESO-1 expressing A375 cell lines prior to
765 cryopreservation.

766 ## IFN$_\gamma$ ELISAs

767 Supernatants were collected at 24 hours post CD8$^+$ T-cell and A375 co-culture, and IFN$_\gamma$
768 secretion from CD8$^+$ T-cells into the culture supernatant was assessed by ELISA as per
769 manufacturer's instructions (Biolegend, #430101). Supernatants were either used fresh in
770 ELISAs, or were stored at -20°C prior to analysis but were never freeze-thawed.

CyTOF sample preparation and data analysis

A375 cells were plated in 96-well flat-bottom plates at 5×10^4 cells per well and pulsed with gp100 peptide (10µg/mL) for a minimum of 4 hours. After peptide loading, cells were washed once with PBS and either incubated with the bispecific T-cell engager at a final concentration of 10^{-10}M or left untreated. Where applicable, bispecific binding was allowed to proceed for at least 30 minutes at 37 °C prior to initiation of the experiment.

Isolated $CD8^+$ T cells were subsequently added to either gp100-pulsed bispecific-coated (stimulated) or uncoated (unstimulated) A375 cells and centrifuged (500 g, 1 min) to promote cell contact and initiate activation. At the end of the time course, cells were transferred to 96-well U-bottom plates, pelleted in ice-cold PBS (1800 rpm, 3 min), and fixed in 100 µl of 1.6% PFA. Fixation was carried out at 4 °C for a minimum of 20 minutes, followed by three washes with 200 µl PBS.

Mass cytometric analysis was performed as previously described. Briefly, dead cells were labelled with 0.25 mM ^{194}Cisplatin (Standard BioTools, Cat# 201194), after which cells were incubated overnight at 4 °C with thiol-reactive barcodes. Excess barcodes were quenched using 2 mM GSH and samples were pooled. Cells were then washed in cell staining buffer (CSB; Standard BioTools, Cat# 201068) and stained with extracellular rare-earth metal-conjugated antibodies for 30 minutes at room temperature. Cells were then permeabilised with 0.1% (v/v) Triton X-100/PBS and 50% methanol/PBS prior to staining with intracellular rare-earth metal-conjugated antibodies for 30 minutes at room temperature. Antibodies were cross-linked using 1.6% (v/v) FA/PBS for 10 minutes. Cells were subsequently incubated overnight at 4 °C with 125 nM ^{191}Ir/^{193}Ir DNA intercalator, washed, resuspended in CAS+ supplemented with 2 mM EDTA, and analysed on a CyTOF XT at 200–400 events per second.

Signal intensities were measured by CyTOF at 1, 5, 10, 15, 30, 45, 60, and 120 minutes post-stimulation using a panel of 42 markers. Raw data were preprocessed in FlowJo and

796 subsequently analysed using the CyGNAL python package (github.com/TAPE-
797 Lab/CyGNAL(*14*)) with default settings.

798 Analysis of published RNA expression and CRISPR dataset

799 To obtain the lists of signalome genes that were regulated during T cell activation, raw counts
800 of bulk RNA sequencing dataset were downloaded from Gene Expression Omnibus (GEO).
801 We filtered the data for CD8+ T cells except for GSE197067, where only pan-T cells were
802 analyzed. Gene IDs were mapped to gene names by mygene package (Python). Data was
803 prefiltered by subsetting for genes that have at least 10 counts in more than 20% of samples.
804 Differential expression analysis was performed using DESeq2 (R)(*49*) using appropriate
805 model design for study and p values were obtained with the wald test. Log fold change (LFC)
806 was shrunk with the apeglm method to reduce inflation of lowly expressed genes. Differentially
807 expressed genes (DEGs) were obtained by thresholding for adjusted p-value < 0.001, and
808 LFC < 1.5. DEGs of different conditions (e.g. timepoints) of the same dataset were merged by
809 their union and intersected with our signalome gene list. To obtain the lists of signalome genes
810 that were identified as hits in pooled CRISPR screening, we downloaded the processed result
811 files from each study, thresholded the hits following the description of each study and
812 intersected with our signalome gene list.
813
814

References

1. B. M. Invergo, P. Beltrao, Reconstructing phosphorylation signalling networks from quantitative phosphoproteomic data. Essays Biochem. 62, 525–534 (2018).
2. E. J. Needham, B. L. Parker, T. Burykin, D. E. James, S. J. Humphrey, Illuminating the dark phosphoproteome. Sci. Signal. 12, eaau8645 (2019).
3. M. Locard-Paulet, G. Voisinne, C. Froment, M. Goncalves Menoita, Y. Ounoughene, L. Girard, C. Gregoire, D. Mori, M. Martinez, H. Luche, J. Garin, M. Malissen, O. Burlet-Schiltz, B. Malissen, A. Gonzalez de Peredo, R. Roncagalli, LymphoAtlas: a dynamic and integrated phosphoproteomic resource of TCR signaling in primary T cells reveals ITSN2 as a regulator of effector functions. Mol. Syst. Biol. 16, e9524 (2020).
4. R. N. Joshi, N. A. Binai, F. Marabita, Z. Sui, A. Altman, A. J. R. Heck, J. Tegnér, A. Schmidt, Phosphoproteomics reveals regulatory T cell-mediated DEF6 dephosphorylation that affects cytokine expression in human conventional T cells. Front. Immunol. 8, 1163 (2017).
5. P. Ruperez, A. Gago-Martinez, A. L. Burlingame, J. A. Oses-Prieto, Quantitative phosphoproteomic analysis reveals a role for serine and threonine kinases in the cytoskeletal reorganization in early T cell receptor activation in human primary T cells. Mol. Cell. Proteomics 11, 171–186 (2012).
6. R. B. Kitata, W.-K. Choong, C.-F. Tsai, P.-Y. Lin, B.-S. Chen, Y.-C. Chang, A. I. Nesvizhskii, T.-Y. Sung, Y.-J. Chen, A data-independent acquisition-based global phosphoproteomics system enables deep profiling. Nat. Commun. 12, 2539 (2021).
7. P. Mertins, NCI CPTAC, D. R. Mani, K. V. Ruggles, M. A. Gillette, K. R. Clauser, P. Wang, X. Wang, J. W. Qiao, S. Cao, F. Petralia, E. Kawaler, F. Mundt, K. Krug, Z. Tu, J. T. Lei, M. L. Gatza, M. Wilkerson, C. M. Perou, V. Yellapantula, K.-L. Huang, C. Lin, M. D. McLellan, P. Yan, S. R. Davies, R. R. Townsend, S. J. Skates, J. Wang, B. Zhang, C. R. Kinsinger, M. Mesri, H. Rodriguez, L. Ding, A. G. Paulovich, D. Fenyö, M. J. Ellis, S. A. Carr, Proteogenomics connects somatic mutations to signalling in breast cancer. Nature 534, 55–62 (2016).
8. V. Cordo', M. T. Meijer, R. Hagelaar, R. R. de Goeij-de Haas, V. M. Poort, A. A. Henneman, S. R. Piersma, T. V. Pham, K. Oshima, A. A. Ferrando, G. J. R. Zaman, C. R. Jimenez, J. P. P. Meijerink, Phosphoproteomic profiling of T cell acute lymphoblastic leukemia reveals targetable kinases and combination treatment strategies. Nat. Commun. 13, 1048 (2022).
9. A. Subramanian, R. Narayan, S. M. Corsello, D. D. Peck, T. E. Natoli, X. Lu, J. Gould, J. F. Davis, A. A. Tubelli, J. K. Asiedu, D. L. Lahr, J. E. Hirschman, Z. Liu, M. Donahue, B. Julian, M. Khan, D. Wadden, I. C. Smith, D. Lam, A. Liberzon, C. Toder, M. Bagul, M. Orzechowski, O. M. Enache, F. Piccioni, S. A. Johnson, N. J. Lyons, A. H. Berger, A. F. Shamji, A. N. Brooks, A. Vrcic, C. Flynn, J. Rosains, D. Y. Takeda, R. Hu, D. Davison, J. Lamb, K. Ardlie, L. Hogstrom, P. Greenside, N. S. Gray, P. A. Clemons, S. Silver, X. Wu, W.-N. Zhao, W. Read-Button, X. Wu, S. J. Haggarty, L. V. Ronco, J. S. Boehm, S. L. Schreiber, J. G. Doench, J. A. Bittker, D. E. Root, B. Wong, T. R. Golub, A next generation Connectivity Map: L1000 platform and the first 1,000,000 profiles. Cell 171, 1437–1452.e17 (2017).
10. S. Ibáñez-Molero, J. T. M. Pruijs, A. Atmopawiro, F. Wang, A. M. Terry, M. Altelaar,

D. S. Peeper, K. E. Stecker, Phosphoprotein dynamics of interacting T cells and tumor cells by HySic. Cell Rep. 43, 113598 (2024).

11. M. N. Navarro, J. Goebel, C. Feijoo-Carnero, N. Morrice, D. A. Cantrell, Phosphoproteomic analysis reveals an intrinsic pathway for the regulation of histone deacetylase 7 that controls the function of cytotoxic T lymphocytes. Nat. Immunol. 12, 352–361 (2011).

12. G. Franciosa, A. W. P. Jensen, A. Martinez-Val, I. Piga, M. Donia, J. V. Olsen, The proteomics and phosphoproteomics landscape of melanoma under T cell attack, bioRxiv (2025). https://doi.org/10.1101/2025.09.12.675787.

13. A. S. Tocheva, M. Peled, M. Strazza, K. R. Adam, S. Lerrer, S. Nayak, I. Azoulay-Alfaguter, C. J. R. Foster, E. A. Philips, B. G. Neel, B. Ueberheide, A. Mor, Quantitative phosphoproteomic analysis reveals involvement of PD-1 in multiple T cell functions. J. Biol. Chem. 295, 18036–18050 (2020).

14. J. Sufi, X. Qin, F. C. Rodriguez, Y. J. Bu, P. Vlckova, M. R. Zapatero, M. Nitz, C. J. Tape, Multiplexed single-cell analysis of organoid signaling networks. Nat. Protoc. 16, 4897–4918 (2021).

15. C. B. Nattress, R. O'Sullivan, D. Fowler, C. Hutton, P. Vlckova, J. Sufi, M. Buschhaus, E. Basiarz, M. Ramos Zapatero, F. Cardoso Rodriguez, X. Qin, A. Campbell, A. Kanouta, V. S. W. Li, K. Chester, J. Anderson, M. Barisa, J. P. H. Fisher, C. J. Tape, Phenoscaping reveals multimodal γδ T-cell cytotoxicity as a strategy to overcome cancer cell-mediated immunomodulation. Cancer Res. 85, 4415–4432 (2025).

16. X. Qin, F. Cardoso Rodriguez, J. Sufi, P. Vlckova, J. Claus, C. J. Tape, An oncogenic phenoscape of colonic stem cell polarization. Cell 186, 5554–5568.e18 (2023).

17. S. Krishnaswamy, M. H. Spitzer, M. Mingueneau, S. C. Bendall, O. Litvin, E. Stone, D. Pe'er, G. P. Nolan, Systems biology. Conditional density-based analysis of T cell signaling in single-cell data. Science 346, 1250689 (2014).

18. M. Kotowski, D. F. Heraghty, M. Körbel, D. Banik, Z. Zhang, S. Kedia, B. Fu, J. McColl, B. Li, J. Clarke, M. Fellermeyer, Y. Lui, G. Bossi, D. K. Cole, H. Chen, E. Basiarz, S. Sharma, E. Petsalaki, C. J. Tape, B. de Wet, S. F. Lee, A. M. Santos, D. Klenerman, S. J. Davis, T-cell signaling relies on partial CD45-exclusion at sub-micron sized cellular contacts, bioRxiv (2025). https://www.biorxiv.org/content/10.1101/2025.08.29.673015v1.

19. N. Moret, C. Liu, B. M. Gyori, J. A. Bachman, A. Steppi, C. Hug, R. Taujale, L.-C. Huang, M. E. Berginski, S. M. Gomez, N. Kannan, P. K. Sorger, Exploring the understudied human kinome for research and therapeutic opportunities, bioRxiv (2020); https://doi.org/10.37473/fic/10.1101/2020.04.02.022277

20. D. van der Meer, S. Barthorpe, W. Yang, H. Lightfoot, C. Hall, J. Gilbert, H. E. Francies, M. J. Garnett, Cell Model Passports-a hub for clinical, genetic and functional datasets of preclinical cancer models. Nucleic Acids Res. 47, D923–D929 (2019).

21. M. Kanehisa, M. Furumichi, Y. Sato, Y. Matsuura, M. Ishiguro-Watanabe, KEGG: biological systems database as a model of the real world. Nucleic Acids Res. 53, D672–D677 (2025).

22. N. G. Bediaga, H. D. Coughlan, T. M. Johanson, A. L. Garnham, G. Naselli, J. Schröder, L. G. Fearnley, E. Bandala-Sanchez, R. S. Allan, G. K. Smyth, L. C. Harrison, Multi-level remodelling of chromatin underlying activation of human T

cells. Sci. Rep. 11, 528 (2021).

23. J. Ogando, M. E. Sáez, J. Santos, C. Nuevo-Tapioles, M. Gut, A. Esteve-Codina, S. Heath, A. González-Pérez, J. M. Cuezva, R. A. Lacalle, S. Mañes, PD-1 signaling affects cristae morphology and leads to mitochondrial dysfunction in human CD8+ T lymphocytes. J. Immunother. Cancer 7, 151 (2019).

24. M. Rade, S. Böhlen, V. Neuhaus, D. Löffler, C. Blumert, M. Merz, U. Köhl, S. Dehmel, K. Sewald, K. Reiche, A time-resolved meta-analysis of consensus gene expression profiles during human T-cell activation. Genome Biol. 24, 287 (2023).

25. Y. Lui, E. Jenkins, E. Z. Q. Ng, M. Kotowski, S. J. Mullin, J. Clarke, S. J. Davis, A. M. Santos, S. Sharma, Cell state and transcription factor modulation during extended ex-vivo CD8+ T-cell expansion, bioRxiv. (2024). https://www.biorxiv.org/content/10.1101/2024.07.17.603780v1.full.

26. S. Sharma, T. Whitehead, M. Kotowski, E. Z. Q. Ng, J. Clarke, J. Leitner, Y.-L. Chen, A. M. Santos, P. Steinberger, S. J. Davis, A high-throughput two-cell assay for interrogating inhibitory signaling pathways in T cells. Life Sci Alliance 7 (2024).

27. E. Shifrut, J. Carnevale, V. Tobin, T. L. Roth, J. M. Woo, C. T. Bui, P. J. Li, M. E. Diolaiti, A. Ashworth, A. Marson, Genome-wide CRISPR Screens in Primary Human T Cells Reveal Key Regulators of Immune Function. Cell 175, 1958–1971.e15 (2018)

28. J. Carnevale, E. Shifrut, N. Kale, W. A. Nyberg, F. Blaeschke, Y. Y. Chen, Z. Li, S. P. Bapat, M. E. Diolaiti, P. O'Leary, S. Vedova, J. Belk, B. Daniel, T. L. Roth, S. Bachl, A. A. Anido, B. Prinzing, J. Ibañez-Vega, S. Lange, D. Haydar, M. Luetke-Eversloh, M. Born-Bony, B. Hegde, S. Kogan, T. Feuchtinger, H. Okada, A. T. Satpathy, K. Shannon, S. Gottschalk, J. Eyquem, G. Krenciute, A. Ashworth, A. Marson, RASA2 ablation in T cells boosts antigen sensitivity and long-term function. Nature 609, 174–182 (2022)

29. R. Schmidt, Z. Steinhart, M. Layeghi, J. W. Freimer, R. Bueno, V. Q. Nguyen, F. Blaeschke, C. J. Ye, A. Marson, CRISPR activation and interference screens decode stimulation responses in primary human T cells. Science 375, eabj4008 (2022).

30. J. Cabezas-Caballero, A. Huhn, M. A. Kutuzov, V. Andre, A. Shomuradova, B. W. A. Peeters, G. M. Gillespie, P. A. van der Merwe, O. Dushek, Generation of T cells with reduced off-target cross-reactivities by engineering co-signalling receptors. Nat. Biomed. Eng., doi: 10.1038/s41551-025-01563-w (2026)

31. S. J. Davis, P. A. van der Merwe, Lck and the nature of the T cell receptor trigger. Trends Immunol. 32, 1–5 (2011).

32. E. Güç, A. Treveil, E. Leach, A. Broomfield, A. Camera, J. Clubley, P. Nieto Garcia, A. Kazachenka, R. Khanolkar, L. Del Carpio, H. Heyn, J. C. Hassel, J. J. Sacco, S. Stanhope, L. Collins, J. M. Piulats, K. Ranade, A. Benlahrech, Tebentafusp, a T cell engager, promotes macrophage reprogramming and in combination with IL-2 overcomes macrophage immunosuppression in cancer. Nat. Commun. 16, 2374 (2025).

33. J. Harper, K. J. Adams, G. Bossi, D. E. Wright, A. R. Stacey, N. Bedke, R. Martinez-Hague, D. Blat, L. Humbert, H. Buchanan, G. S. Le Provost, Z. Donnellan, R. J. Carreira, S. J. Paston, L. U. Weigand, M. Canestraro, J. P. Sanderson, S. Botta Gordon-Smith, K. L. Lowe, K. A. Rygiel, A. S. Powlesland, A. Vuidepot, N. J. Hassan, B. J. Cameron, B. K. Jakobsen, J. Dukes, An approved in vitro approach to preclinical safety and efficacy evaluation of engineered T cell receptor anti-CD3

bispecific (ImmTAC) molecules. PLoS One 13, e0205491–e0205491 (2018).
34. J. E. Purvis, G. Lahav, Encoding and decoding cellular information through signaling dynamics. Cell 152, 945–956 (2013).
35. M. J. Harris, M. Fuyal, J. R. James, Quantifying persistence in the T-cell signaling network using an optically controllable antigen receptor. Mol. Syst. Biol. 17, e10091 (2021).
36. S. C. Bendall, E. F. Simonds, P. Qiu, E.-A. D. Amir, P. O. Krutzik, R. Finck, R. V. Bruggner, R. Melamed, A. Trejo, O. I. Ornatsky, R. S. Balderas, S. K. Plevritis, K. Sachs, D. Pe'er, S. D. Tanner, G. P. Nolan, Single-cell mass cytometry of differential immune and drug responses across a human hematopoietic continuum. Science 332, 687–696 (2011).
37. H. Dada, M. L. Dustin, Goldilocks and the three TILs. J. Exp. Med. 219 (2022).
38. V. Horkova, A. Drobek, D. Paprckova, V. Niederlova, A. Prasai, V. Uleri, D. Glatzova, M. Kraller, M. Cesnekova, S. Janusova, E. Salyova, O. Tsyklauri, T. A. Kadlecek, K. Krizova, R. Platzer, K. Schober, D. H. Busch, A. Weiss, J. B. Huppa, O. Stepanek, Unique roles of co-receptor-bound LCK in helper and cytotoxic T cells. Nat. Immunol. 24, 174–185 (2023).
39. T. Pawson, J. D. Scott, Signaling through scaffold, anchoring, and adaptor proteins. Science 278, 2075–2080 (1997).
40. T. Pawson, P. Nash, Assembly of cell regulatory systems through protein interaction domains. Science 300, 445–452 (2003).
41. W. A. Lim, T. Pawson, Phosphotyrosine signaling: evolving a new cellular communication system. Cell 142, 661–667 (2010).
42. D. Detilleux, P. Raynaud, B. Pradet-Balade, D. Helmlinger, The TRRAP transcription cofactor represses interferon-stimulated genes in colorectal cancer cells. Elife 11, e69705 (2022).
43. M. Li, L. Chen, F. Yu, H. Mei, X. Ma, K. Ding, Y. Yang, Z. Rong, CTDSPL2 promotes the progression of non-small lung cancer through PI3K/AKT signaling via JAK1. Cell Death Discov. 10, 389 (2024).
44. S. Jutz, A. Hennig, W. Paster, Ö. Asrak, D. Dijanovic, F. Kellner, W. F. Pickl, J. B. Huppa, J. Leitner, P. Steinberger, A cellular platform for the evaluation of immune checkpoint molecules. Oncotarget 8, 64892–64906 (2017).
45. Y.-L. Chen, J. S. W. Ng, R. Ottakandathil Babu, J. Woo, J. Nahler, C. S. Hardman, P. Kurupati, L. Nussbaum, F. Gao, T. Dong, K. Ladell, D. A. Price, D. A. Duncan, D. Johnson, U. Gileadi, H. Koohy, G. S. Ogg, Group A Streptococcus induces CD1a-autoreactive T cells and promotes psoriatic inflammation. Sci. Immunol. 8, eadd9232 (2023).
46. S. Sharma, G. J. Wright, Cell Surface Receptor Identification Using Genome-Scale CRISPR/Cas9 Genetic Screens (2020; https://www.jove.com/t/60803/cell-surface-receptor-identification-using-genome-scale-crisprcas9).
47. M. Aleksic, O. Dushek, H. Zhang, E. Shenderov, J.-L. Chen, V. Cerundolo, D. Coombs, P. A. van der Merwe, Dependence of T cell antigen recognition on T cell receptor-peptide MHC confinement time. Immunity 32, 163–174 (2010).
48. H. W. Borchers, Pracma: Practical Numerical Math Functions (https://cran.r-project.org/web/packages/pracma/index.html).
49. M. I. Love, W. Huber, S. Anders, Moderated estimation of fold change and dispersion for RNA-seq data with DESeq2, bioRxiv (2014). https://doi.org/10.1101/002832.

Author contribution:

The experiments were conceived by S.S, E.P, S.J.D, and C.J.T, and the methodology developed by J.C and S.S. The experimental work was undertaken by J.C, S.S, C.T.G, E.B, M.K, A.M.S, M.T. V, P.S, J.X.L. Data analysis was performed by J.C, H.C, and S.S. The work was supervised by S.S, E.P, S.J.D, C.J.T, and funding was acquired by J.C, S.S, E.P, S.J.D, C.J.T. The original manuscript was written by J.C, S.S, and E.P and revised by H.C, M.K, A.M.S, C.J.T and S.J.D.

Acknowledgements

This work was funded by MRC (grant MR/W025507/1 to E.P., S.S., C.T., and S.J.D.) and Wellcome grant to S.S (317519/Z/24/Z), and MSIF pump priming grant to J.C (BRDNB420).